Geophysical Research Letters

RESEARCH LETTER
10.1029/2023GL105277

**Key Points:**

- The El Niño/Southern Oscillation-induced Pacific-North American (PNA) teleconnection pattern is farther westward during La Niña relative to that in El Niño
- The nonlinear energy advection redistributes the kinetic energy, hence contributing to the asymmetric PNA teleconnections
- Different synoptic-scale transient eddy activities help to maintain and amplify the asymmetry through a feedback effect

**Supporting Information:**

Supporting Information may be found in the online version of this article.

**Correspondence to:**

G. Huang and K. Hu,
hg@mail.iap.ac.cn;
hkm@mail.iap.ac.cn

**Citation:**

Wang, Y., Hu, K., Huang, G., & Tao, W. (2023). The role of nonlinear energy advection in forming asymmetric structure of ENSO teleconnections over the North Pacific and North America. *Geophysical Research Letters*, *50*, e2023GL105277. https://doi.org/10.1029/2023GL105277

Received 6 JUL 2023
Accepted 28 AUG 2023



# The Role of Nonlinear Energy Advection in Forming Asymmetric Structure of ENSO Teleconnections Over the North Pacific and North America

**Ya Wang[1], Kaiming Hu[1,2,3], Gang Huang[1,2,4], and Weichen Tao[1]**

[1]State Key Laboratory of Numerical Modeling for Atmospheric Sciences and Geophysical Fluid Dynamics, Institute of Atmospheric Physics, Chinese Academy of Sciences, Beijing, China, [2]Laboratory for Regional Oceanography and Numerical Modeling, Qingdao National Laboratory for Marine Science and Technology, Qingdao, China, [3]Collaborative Innovation Center on Forecast and Evaluation of Meteorological Disasters (CIC-FEMD), Nanjing University of Information Science & Technology, Nanjing, China, [4]College of Earth and Planetary Sciences, University of Chinese Academy of Sciences, Beijing, China

**Abstract** In boreal winter, the El Niño/Southern Oscillation (ENSO)-induced Pacific-North American (PNA) teleconnection pattern is farther westward during La Niña relative to that in El Niño, causing discernible distinct climate implications. However, there has been a lack of consensus regarding the underlying mechanism driving this asymmetric structure. This study highlights the contribution of nonlinear kinetic energy advection (nKA) to this asymmetry. The zonally symmetric responses to ENSO, specifically the anomalies in zonal mean zonal flow, generate opposing nKA patterns by advecting anomalous eddy kinetic energy in the North Pacific, which leads to the shift of the PNA teleconnection pattern. In addition to nKA, transient eddy activities responded to changes of baroclinicity help maintain the asymmetry through a feedback effect. These findings underscore the importance of considering extratropical factors, such as nonlinear energy processes and synoptic-scale transient eddies, in understanding the mechanism responsible for the asymmetric structure of the PNA teleconnection pattern.

**Plain Language Summary** The El Niño/Southern Oscillation (ENSO)-induced atmospheric anomalies over the North Pacific and North America (PNA region) are more westward during La Niña relative to that during El Niño in boreal winter. The disparity of atmospheric responses causes discernible distinct climate implications, and limits the seasonal prediction. The mechanism underlying this asymmetry, however, remains in disagreement. Some believe that it is due to variations in the location of tropical convective anomalies. Whereas others show that the climatological zonal flow could anchor the disturbance. Utilizing a more comprehensive energy diagnostic framework, we find that the nonlinear component, in particular, the nonlinear kinetic energy advection and the feedback effect of synoptic-scale disturbances contribute to the asymmetric atmospheric responses. The study emphasizes the importance of nonlinear processes and multi-scale interactions in the asymmetric structure of ENSO-induced atmospheric anomalies in the PNA region, which are essential for understanding ENSO teleconnections, comprehending model biases, and improving seasonal predictions.

## 1. Introduction

The El Niño/Southern Oscillation (ENSO), as the dominant interannual air-sea coupled mode in the tropical Pacific, significantly impacts global climate variability (Adames & Wallace, 2017; Cai et al., 2019; Ciasto et al., 2015; Held & Kang, 1987; Held et al., 2002; Hoerling et al., 1997; Horel & Wallace, 1981a, 1981b; Johnson & Kosaka, 2016; Tao et al., 2016; Xie et al., 2009). One of the strongest and most notable features of ENSO is the ENSO-forced Pacific-North American (PNA) teleconnection pattern observed during boreal winter. This pattern exhibits a wave structure extending from the tropical Pacific to North America, influencing the strength of Aleutian Low and the high-pressure center in western Canada, thereby leading to extreme weather and climate events across North America (Hoerling et al., 1997; Horel & Wallace, 1981a, 1981b; Johnson & Kosaka, 2016; Liu & Alexander, 2007; Trenberth et al., 1998). However, simulating and predicting the PNA teleconnection pattern, despite its significance and predictability, face challenges due to inadequate understanding and simulation of its complex nonlinear characteristics (Kim et al., 2021). One particular aspect that presents difficulties is the asymmetry observed in the PNA teleconnection pattern. During El Niño (EN), the teleconnection wave

train exhibits an eastward shift relative to that in La Niña (LN; Hoerling et al., 1997; Y. Wang et al., 2021). Contemporary climate models struggle to accurately represent this asymmetry, which hampers reliable predictions (Kim et al., 2021). Various studies have aimed to identify the cause of this asymmetry. Some attribute it to variations in the location of tropical convective anomalies between EN and LN (e.g., Hoerling et al., 1997), while others suggest that the extratropical climatological circulation, specifically the subtropical jet stream (STJ), may influence the position of disturbances by modifying the barotropic energy conversion in the exit zone of the STJ (Simmons et al., 1983; Y. Wang et al., 2022a, 2022b; Zhou et al., 2020). Via a hierarchy of linear model experiments, Simmons et al. (1983) demonstrated that the stationary Rossby wave train undergoes minimal movement when tropical convection varies, as long as the background circulation remains unchanged. These differing interpretations contribute to ongoing disagreements concerning the asymmetry's explanation.

While the PNA teleconnection pattern constitutes a zonally asymmetric component of the atmospheric response to ENSO, there are also significant zonally symmetric components (Held et al., 2002; Seager et al., 2003), including changes in tropical tropospheric temperature and STJ in both hemispheres (Held et al., 2002; Seager et al., 2003). During EN, the tropical troposphere exhibits above-normal temperatures across all longitudes, and the STJ strengthens on their equatorward flanks in the North Hemisphere. The opposite occurs during LN. Simmons et al. (1983) demonstrated that the PNA teleconnection pattern is highly determined by the background flows. This raises the question of whether the zonally symmetric response to ENSO affects the PNA teleconnection pattern by altering the background flows. In this study, we seek to answer this question by incorporating nonlinear effects into a comprehensive energy diagnostic equation. We show that the kinetic energy advected by the zonally symmetric responses is critical for establishing the asymmetric structure of the ENSO-induced PNA teleconnection pattern. Furthermore, the feedback effect of synoptic-scale transient eddies helps maintain this asymmetry.

The rest of this study is organized as follows: Section 2 introduces data and models. Section 3 presents the mechanism leading to the asymmetry based on an energy diagnostic framework. Finally, Section 4 provides a summary.

## 2. Data and Methods

### 2.1. Data

In this study, we collected daily and monthly mean geopotential height, zonal and meridional winds from the National Centers for Environmental Prediction-Department of Energy Atmospheric Reanalysis 2 (NCEP2; Kanamitsu et al., 2002) at a resolution of 2.5° × 2.5° for the period 1979 to 2015. The global gridded monthly sea surface temperature (SST) data sets from Extended Reconstructed SST (ERSST.v5 SST) are utilized (Huang et al., 2017). To track ENSO occurrences, the December-January-February (DJF) mean Niño3.4 (5°S–5°N, 170°–120°W) SST index is employed. An EN (A LN) event arises when the DJF Niño3.4 index exceeds (falls below) 0.5 (−0.5) °C. The study employs composite analysis and the statistical significance is determined using the two-tailed Student's *t*-test.

### 2.2. Models

We employ the ECHAM5.3.2 atmospheric general circulation model (AGCM) developed by the Max Planck Institute for Meteorology for AGCM simulations. The model has a triangular truncation at zonal wave-number 63 (T63; equivalent to a horizontal resolution of 1.9°) and 31 vertical levels. Roeckner et al. (2003) provide more information about this model. Additionally, we use a T42L20 dry version of the linear baroclinic model (LBM) based on the primitive equations linearized at a given state. The model has a horizontal resolution of T42 and 20 sigma levels, and schemes for horizontal and vertical diffusion, Rayleigh friction, and Newtonian damping. Watanabe and Kimoto (2000) provide a detailed introduction to the model. To obtain a stable atmospheric response to the heating forcing, we integrate the model for 50 days and use the averages from 20 to 50 days.

### 2.3. Eddy Kinetic Energy Tendency

In this study, we utilize the complete eddy kinetic energy tendency equation (Equation 1) for energy diagnostic. This equation could be obtained from the momentum equation; Supporting Information S1 gives a detailed derivation of the formula. EKE is the eddy kinetic energy, $u'$, $v'$, $\omega'$, $T'$ and $\Phi'$ are the anomalous monthly zonal wind,

meridional wind, vertical wind, temperature, and geopotential, respectively, $\overline{u}$ and $\overline{v}$ represent the background zonal and meridional flow. KI represents the kinetic energy extracted from the basic flow, while the conversion from anomalous effective potential energy to anomalous kinetic energy is represented by KP. The combination of KP and KI forms as the energy source of the disturbance. KA describes the kinetic energy advected by the basic flow and the anomalous wind, which could be seen as the redistribution term. This term could be further decomposed to linear KA (lKA $= -\left[\overline{u}\frac{\partial \mathrm{EKE}}{\partial x} + \overline{v}\frac{\partial \mathrm{EKE}}{\partial y} + \overline{\omega}\frac{\partial \mathrm{EKE}}{\partial p}\right]$) and nonlinear KA (nKA $= -\left[u'\frac{\partial \mathrm{EKE}}{\partial x} + v'\frac{\partial \mathrm{EKE}}{\partial y} + \omega'\frac{\partial \mathrm{EKE}}{\partial \mathrm{p}}\right]$). The generation of the EKE by local convergence of the eddy geopotential flux is given by KZ. Equation 1 is similar to Lau and Lau (1992), except that a time-mean operator is added in each term in Lau and Lau (1992) analyses, as it was used to diagnosis the transient eddy kinetic energy balance. KI in Equation 1 equals CK ($-\left[u'v'\left(\frac{\partial \overline{u}}{\partial y} + \frac{\partial \overline{v}}{\partial x}\right) + \frac{1}{2}\left(\frac{\partial \overline{v}}{\partial y} - \frac{\partial \overline{u}}{\partial x}\right)\left(v'^2 - u'^2\right)\right]$) given the assumption that there is no divergence in the mean flow (see Supporting Information S1 for detailed derivation), and the latter is widely used for energy diagnostic for Rossby waves (e.g., Kosaka & Nakamura, 2006). Energy analysis has been widely used to diagnose the position of key climate systems, as represented by geopotential height or wind fields. For instance, Simmons et al. (1983) investigated how background mean flow modulated wave trains triggered by tropical heating using kinetic energy conversion. Kosaka and Nakamura (2006) examined the relationship between mean flow and the Pacific-Japan teleconnection pattern utilizing barotropic and baroclinic energy conversion.

$$\begin{aligned}\frac{\partial \mathrm{EKE}}{\partial t} = &\underbrace{-\left[u'^2\frac{\partial \overline{u}}{\partial x} + u'v'\left(\frac{\partial \overline{u}}{\partial y} + \frac{\partial \overline{u}}{\partial x}\right) + v'^2\frac{\partial \overline{v}}{\partial y} + u'\omega'\frac{\partial \overline{u}'}{\partial p} + v'\omega'\frac{\partial \overline{v}}{\partial p}\right]}_{\mathrm{KI}} \\ &\underbrace{-(u'+\overline{u})\left(\frac{\partial \mathrm{EKE}}{\partial x}\right) - (v'+\overline{v})\left(\frac{\partial \mathrm{EKE}}{\partial y}\right) + (\omega'+\overline{\omega})\left(\frac{\partial \mathrm{EKE}}{\partial P}\right)}_{KA} \\ &\underbrace{-\frac{R}{P}\omega'T'}_{\mathrm{KP}} \underbrace{- u'\frac{\partial \Phi'}{\partial x} - v'\frac{\partial \Phi'}{\partial y} - \omega'\frac{\partial \Phi'}{\partial P}}_{\mathrm{KZ}}.\end{aligned} \tag{1}$$

### 2.4. Synoptic-Scale Transient Eddy-Induced Geopotential Height Tendency

The synoptic-scale transient eddy-induced geopotential height tendency is shown as follows (Lau et al., 2005):

$$\left(\frac{\partial Z}{\partial t}\right)_{\mathrm{eddy}} = \frac{f}{g}\nabla^{-2}\left[-\nabla\cdot\left(\overline{\boldsymbol{V}''\zeta''}\right)\right] \tag{2}$$

where $Z$ is the monthly averaged geopotential height, $g$ is the acceleration of gravity, and $\boldsymbol{V}''$ and $\boldsymbol{\zeta}''$ are the synoptic-scale transient winds and relative vorticity filtered by a band of 2–10 days. The overbar represents the time average of a month.

## 3. Results

### 3.1. The Asymmetric Structure of the PNA Teleconnection Pattern

Figures 1a and 1b shows the boreal winter composite anomalies of 200-hPa geopotential height during EN and LN, respectively. During EN, the anomalous center in the North Pacific is located around 150°W, and the anomalous center over North America is situated in central Canada; whereas during LN, the anomalous center in the North Pacific shifts westward by nearly 10°, and the anomalous center over North America also moves westward, settling in western Canada. These contrasting patterns suggest an asymmetric structure in the atmospheric response to different phases of ENSO. Considering that different phases, SST patterns and intensities of ENSO may all lead to different atmospheric responses, we first analyze the source of this asymmetry through a series of AGCM experiments. The experiments utilized symmetrical SST conditions (Figures 1c and 1d), referred to as EN_SYM_SST and LN_SYM_SST, as proposed by Trascasa-Castro et al. (2019). The symmetrical SST patterns were constructed using a theoretical equation to ensure that the strengths of EN and LN were identical. To assess the asymmetry, we compared the results of these experiments with a control experiment forced with climatological

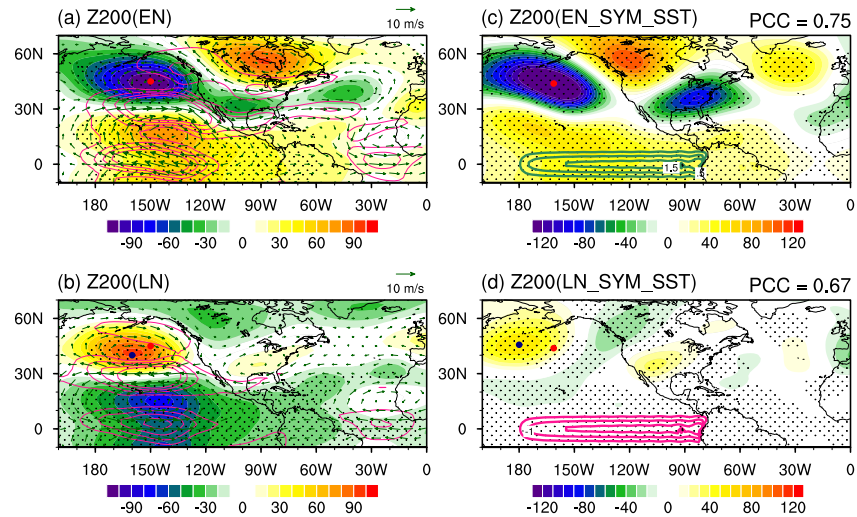


**Figure 1.** DJF composite 200-hPa geopotential height (shading; m), winds (vectors; 10 m/s), and eddy kinetic energy (EKE; contour lines with interval of 10 $m^2/s^2$) anomalies during (a) El Niño (EN) and (b) La Niña (LN) in NCEP2. The red and blue circles represent the central position of the anomalous geopotential height in North Pacific during EN and LN, respectively. Strong El Niño/Southern Oscillation (ENSO) events with Niño3.4 index greater (less) than 1 (−1) °C are selected in this study, as the atmospheric response to strong ENSO events is more pronounced than weak ENSO events. DJF anomalous 200-hPa geopotential height (shading; m) and SST (contour lines; K) during (c) EN and (d) LN in SYM_SST experiments. PCC denote pattern correlation coefficient of the model responses with the corresponding observed composites. Zonal mean anomalies have been to focus on the Pacific-North American teleconnection pattern.

SST data from the period 1980–2005. Model results show a significant asymmetric ENSO-triggered PNA teleconnection pattern between EN_SYM_SST and LN_SYM_SST experiment (Figures 1c and 1d). The result indicates that factors other than the spatial pattern and intensity of SST also contribute to the observed asymmetry in the PNA response. This finding highlights the importance of considering additional factors, such as nonlinear processes and synoptic-scale transient eddies, in understanding the complete mechanism behind the asymmetric PNA teleconnection pattern during different phases of ENSO.

### 3.2. The Role of Nonlinear Energy Advection on the Asymmetry

Next, we employ Equation 1 to explain this phenomenon. Figures 2a and 2b displays the distribution of KI in EN and LN. We first focusing on the energy sources comprised of KI and KP. Significant positive KI distributes in the front of the STJ. According to Simmons et al. (1983), the Pacific STJ exit zone with the confluent zonal wind ($\frac{\partial \bar{u}}{\partial x} \ll 0$; Figure 2a) favors kinetic energy conversion, which facilitates the development of the wave train. Negative KI centered on the flank of the STJ is mainly attributable to $-u'v'\left(\frac{\partial \bar{u}}{\partial y}\right)$, which is highly influenced by the meridional gradient of zonal mean flow ($\frac{\partial \bar{u}}{\partial y}$). Strong negative KP (Figure 2c) anomalies near 20°N in the eastern Pacific are mainly due to the subsidence movement in this region. Su and Neelin (2002) illustrated that anomalous dry advection could induce descent anomalies north of the EN warm SST. Comparing EKE (Figure 1a) to energy sources (KI and KP) reveals that KI primarily contributes to the development of the ENSO-triggered PNA teleconnection pattern, whereas the impact of KP is minor, especially north of 30°N (Figures 2c and 2d). The weak KP likely arises from the quasi-barotropic structure of the PNA pattern (Held et al., 2002), which prevents it from extracting the potential energy from the mean flow. Similar conclusion could be obtained in LN (Figures 2b and 2d).

As the climatological zonal flow keeps fixed, the energy source, KI, does not cause asymmetry. The differences in KI (Figures 2a and 2b) and lKA (Figures 2i and 2j) are mostly attributable to the shift of the disturbances themselves. KP is small in the subtropics and almost canceled out by KZ. Figures 2g–2j show the distribution of nKA, which varies considerably between EN and LN. During EN, a negative and a positive anomaly are alternatively distributed from west to east in the subtropical Pacific. During LN, the eastern disturbance is replaced by a negative anomaly, and the western one become positive, accompanied by a general westward shift of the

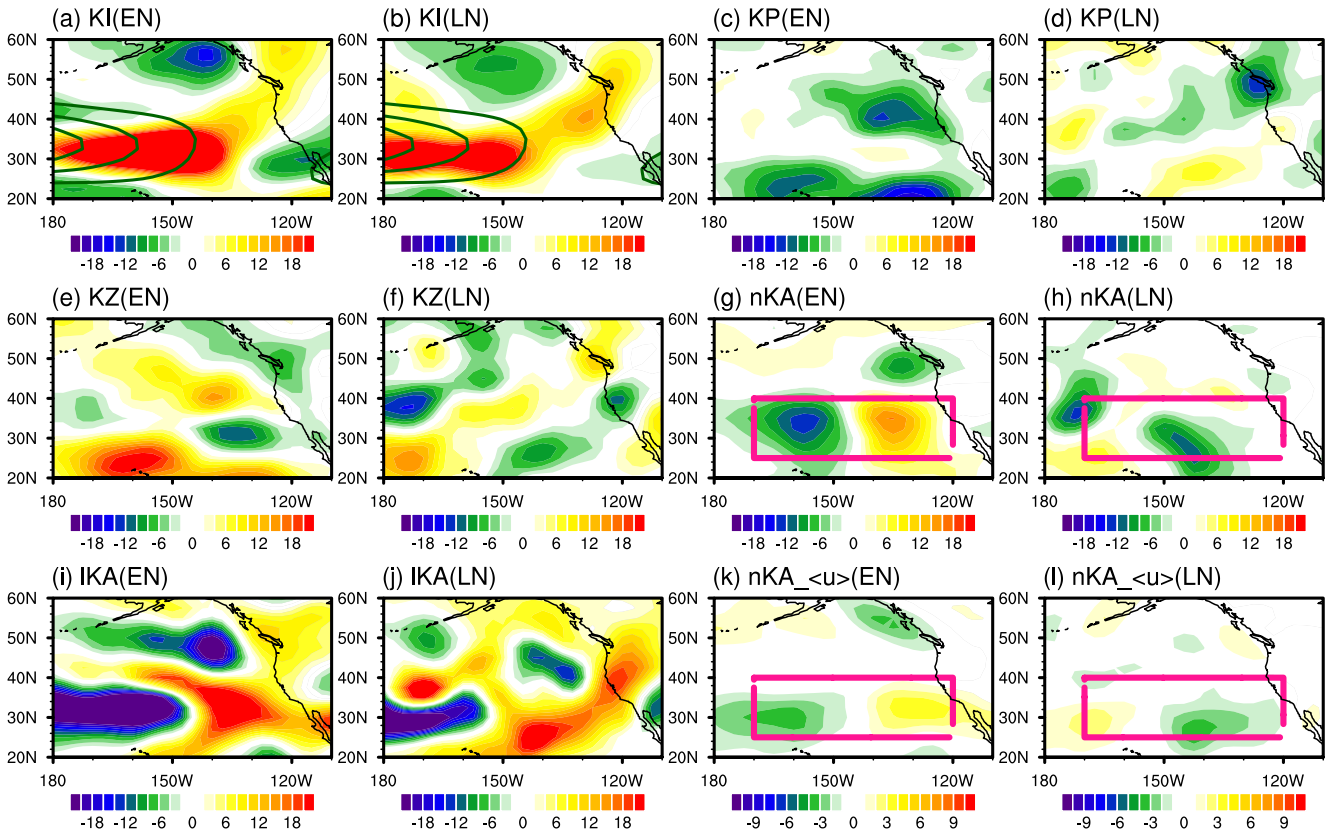


**Figure 2.** Horizontal distribution of composite (a, b) KI ($m^2\ s^{-3}$), (c, d) KP ($m^2\ s^{-3}$), (e, f) KZ ($m^2\ s^{-3}$), (g, h) nKA ($m^2\ s^{-3}$), (i, j) KZ ($m^2\ s^{-3}$), and (k, l) nKA_$\langle u \rangle$ ($m^2\ s^{-3}$) in (a, c, e, g, i, k) El Niño and (b, d, f, h, j, l) La Niña, respectively. The contour lines denote the climatological zonal flow (larger than 30 m/s are shown, with interval of 10 m/s).

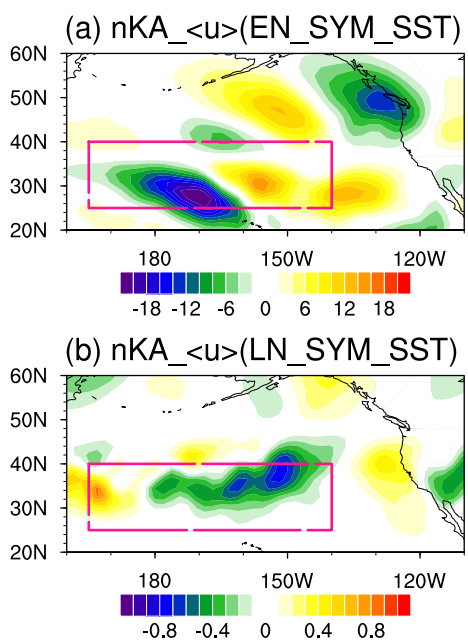


**Figure 3.** Horizontal distribution of nKA_$\langle u \rangle$ ($m^2\ s^{-3}$) in (a) EN_SYM_SST and (b) LN_SYM_SST, respectively.

anomalous centers. The difference in nKA between EN and LN could be partially attributable to the advection by the zonally symmetric response of atmospheric circulation to ENSO. Su et al. (2003) showed that positive tropical SST anomalies warm the tropical tropospheric temperature through moist adiabatic adjustment. The warming increases meridional temperature gradients, leading to anomalous westerlies via the zonally symmetric pathway (Rind et al., 2001; Seager et al., 2003). The zonally symmetric responses, featuring strengthened zonal mean zonal winds during EN, and the opposite during LN are seen in the subtropics (Figure S1 in Supporting Information S1). These anomalous zonal winds would in turn advect eddy kinetic energy, resulting in different nKA distributions during EN and LN, leading to the asymmetric responses of atmospheric circulation to ENSO. As the anomalies in nKA consist of both zonal flow and wave trains, we further calculate nKA_$\langle u \rangle = -\langle u' \rangle \frac{\partial \mathrm{EKE}}{\partial x}$ (where $\langle u' \rangle$ represents the zonal mean zonal flow anomaly) and found that it displays a similar pattern to nKA (Figures 3k and 3l). The magnitude of nKA_$\langle u \rangle$ is somewhat smaller than nKA, implying the interaction between the zonal flow and the quasi-stationary Rossby wave trains may also have some contributions.

Moreover, we further test the proposed mechanism in AGCM experiments. The experimental results, including the zonal mean zonal flow (Figure S2 in Supporting Information S1), nKA (Figure 3) and other energy diagnostic terms (Figure S3 in Supporting Information S1) show similarities to the observations. Zonal mean zonal wind anomalies in model results display a

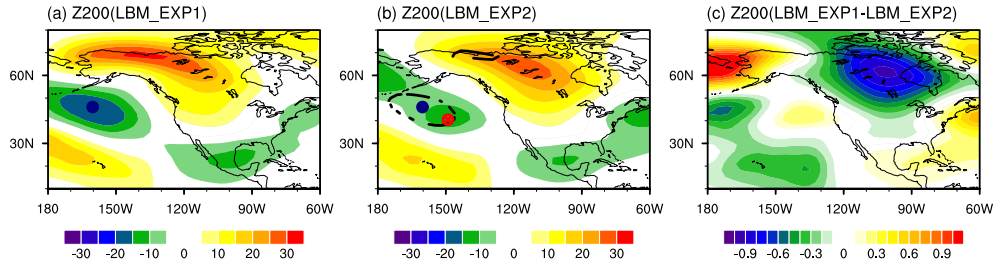


**Figure 4.** Distributions of 200-hPa geopotential height (shading; m) in (a) LBM_EXP1 and (b) LBM_EXP2. (c) Differences between EXP1 and EXP2, where the anomalies are standardized by the absolute value of the central value in the North Pacific. The blue and red circles represent the central position of the anomalous geopotential height in North Pacific in LBM_EXP1 and LBM_EXP2, respectively.

opposite change in LN_SYM_SST relative to EN_SYM_SST (Figure S2 in Supporting Information S1). As in observations, the positive zonal flow anomalies (Figure S2 in Supporting Information S1) in EN_SYM_SST lead to west-negative-east positive nKA anomalies in the subtropical Pacific (Figure 3a). In contrast, the distribution is reversed in LN_SYM_SST, with west-positive-east negative anomalies (Figure 3b). These results in AGCM experiments support the notion that zonal flow anomalies play a crucial role in driving the asymmetric structure of the ENSO-induced PNA teleconnection pattern.

To further validate the effect of anomalous zonal flow on kinetic energy advection and the Rossby wave train, we conducted two sets of LBM experiments. In the first experiment (hereafter referred to LBM_EXP1), we applied a heating source centered at 150°W with a cosine elliptical pattern, a peak of 3 K/day at the 0.45 sigma level, and used the climatological DJF mean flow from 1979 to 2005 in NCEP reanalysis. In the other experiment (LBM_EXP2), we used the same heating source but increased the background zonal wind by 1 m/s compared to LBM_EXP1 to mimic the enhancement of zonal wind during EN events. It is important to note that in LBM_EXP2, the overall increase in zonal flow does not alter the position of the jet exit region and the divergent region of zonal flow, thus not affecting KI. A comparison of the two experiments reveals that the PNA wave train in LBM_EXP2 shifts eastward (Figures 4a and 4b), corresponding to the advection of kinetic energy by anomalous zonal mean zonal flow. Figure S4 in Supporting Information S1 displays the difference of KA contributed by the anomalous background zonal flow, which could be seen as nKA in observations. The results show that an increase in the background zonal flow would lead to a west-negative-east-positive pattern in the subtropical central Pacific, similar to that in observations (Figure 2k). The energy pattern, in turn, would cause the disturbance to develop to the east, as shown in Figure 4b.

### 3.3. The Role of Synoptic-Scale Transient Eddies

In addition to nonlinear energy advection, synoptic-scale transient eddies play a significant role in maintaining the asymmetry through the feedback effect. The divergent or convergent centers of **E** are inconsistent during EN and LN due to differences in anomalous zonal flow and the associated baroclinicity, and this disparity maintains the asymmetries via wave-mean flow interactions. During EN, the prominent divergence of **E** near 150° and 110°W belt suggests strengthened synoptic-scale activity and accelerated westerly winds in this site, whereas **E** convergence on its northern side weakens the zonal flow (Figure S5a in Supporting Information S1). These changes in zonal winds imply an enhanced low-pressure center in the subtropics as in Figure 1a. During LN, the locations of the **E** convergence or divergence are farther westward relative to those in EN (Figure S5b in Supporting Information S1), which has a westward influence on the teleconnection wave train, thereby maintaining the asymmetry between EN and LN.

## 4. Summary

In this paper, we investigate the mechanism of the asymmetric ENSO teleconnections in the PNA region during boreal winter and try to reconcile two different views on the issue. Our findings highlight the significant role of nonlinear energy advection in contributing to the asymmetric structure of the teleconnection wave train.

During EN, a negative and a positive nKA anomaly are alternatively distributed from west to east in the subtropical Pacific. During LN, the eastern disturbance is replaced by a negative anomaly, and the western one becomes

positive, accompanied by a general westward shift of the anomalous centers. The difference in nKA between EN and LN could be partially attributable to the advection by the zonally symmetric response of atmospheric circulation to ENSO. The zonally symmetric responses, featuring strengthened zonal mean zonal wind anomalies during EN, and the opposite during LN, would in turn advect eddy kinetic energy, resulting in different nKA distributions, leading to the asymmetric responses of atmospheric circulation to ENSO. In addition to nonlinear energy advection, synoptic-scale transient eddies also play a role in maintaining the asymmetry through the feedback effect.

Our study underscores the significance of nonlinear processes and multi-scale interactions in understanding the asymmetry of ENSO-forced PNA teleconnection patterns. These findings have implications for improving our understanding of ENSO teleconnections, addressing model biases, and enhancing seasonal predictions. In addition to the zonal asymmetry in ENSO-induced teleconnections, the meridional variations of the PNA teleconnection and asymmetry in non-ENSO-triggered PNA teleconnection patterns also warrant in-depth discussion and could potentially yield insights from a nonlinear energy diagnostics framework. It is important to note that our analysis focused on the energy conversion perspective, other pathways, such as subtropical wave sources (Sardeshmukh & Hoskins, 1988; X. Wang & Yang, 2023; Yeh et al., 2018), and wave propagation (Feng et al., 2016; Lu et al., 2002; Yiu & Maycock, 2020) may also contribute to the wave train influenced by tropical convective anomalies. Exploring the linkages and distinctions between these different pathways will provide a more comprehensive and in-depth understanding of ENSO teleconnections in future research.

## Conflict of Interest

The authors declare no conflicts of interest relevant to this study.

## Data Availability Statement

NCEP2 data (Kanamitsu et al., 2002) could be download from https://psl.noaa.gov/data/gridded/data.ncep.reanalysis.html. The ERSST (Huang et al., 2017) is available at https://doi.org/10.7289/V5T72FNM. The data from the ECHAM and LBM simulations have been made publicly available via a data repository: https://doi.org/10.5281/zenodo.8271667.

**Acknowledgments**
The study is jointly supported by the National Natural Science Foundation of China (41831175, 42141019, 41721004), the Second Tibetan Plateau Scientific Expedition and Research (STEP) program (Grant 2019QZKK0102), the National Natural Science Foundation of China (42175049 and 42175040) and Youth Innovation Promotion Association of CAS (2021072). The authors declare no competing interest. The authors would like to thank the editor and three anonymous reviewers for their comments and suggestions that have helped us improve the final manuscript.

## References

Adames, A. F., & Wallace, J. M. (2017). On the tropical atmospheric signature of El Nino. *Journal of the Atmospheric Sciences*, *74*(6), 1923–1939. https://doi.org/10.1175/jas-d-16-0309.1

Cai, W., Wu, L., Lengaigne, M., Li, T., McGregor, S., Kug, J. S., et al. (2019). Pantropical climate interactions. *Science*, *363*(6430), eaav4236. https://doi.org/10.1126/science.aav4236

Ciasto, L. M., Simpkins, G. R., & England, M. H. (2015). Teleconnections between tropical Pacific SST anomalies and extratropical Southern Hemisphere climate. *Journal of Climate*, *28*(1), 56–65. https://doi.org/10.1175/jcli-d-14-00438.1

Feng, J., Chen, W., & Li, Y. (2016). Asymmetry of the winter extra-tropical teleconnections in the Northern Hemisphere associated with two types of ENSO. *Climate Dynamics*, *48*(7–8), 2135–2151. https://doi.org/10.1007/s00382-016-3196-2

Held, I. M., & Kang, I. S. (1987). Barotropic models of the extratropical response to El-Nino. *Journal of the Atmospheric Sciences*, *44*(23), 3576–3586. https://doi.org/10.1175/1520-0469(1987)044<3576:bmoter>2.0.co;2

Held, I. M., Ting, M. F., & Wang, H. L. (2002). Northern winter stationary waves: Theory and modeling. *Journal of Climate*, *15*(16), 2125–2144. https://doi.org/10.1175/1520-0442(2002)015<2125:nwswta>2.0.co;2

Hoerling, M. P., Kumar, A., & Zhong, M. (1997). El Nino, La Nina, and the nonlinearity of their teleconnections. *Journal of Climate*, *10*(8), 1769–1786. https://doi.org/10.1175/1520-0442(1997)010<1769:enolna>2.0.co;2

Horel, J. D., & Wallace, J. M. (1981a). Planetary-scale atmospheric phenomena associated with the Southern Oscillation. *Monthly Weather Review*, *109*(4), 813–829. https://doi.org/10.1175/1520-0493(1981)109<0813:psapaw>2.0.co;2

Horel, J. D., & Wallace, J. M. (1981b). Planetary-scale atmospheric phenomenon associated with the Southern Oscillation.

Huang, B., Thorne, P. W., Banzon, V. F., Boyer, T., Zhang, H. M., Lawrimore, J. H., et al. (2017). Extended reconstructed sea surface temperature, version 5 (ERSSTv5): Upgrades, validations, and intercomparisons. *Journal of Climate*, *30*(20), 8179–8205. https://doi.org/10.1175/jcli-d-16-0836.1

Johnson, N. C., & Kosaka, Y. (2016). The impact of eastern equatorial Pacific convection on the diversity of boreal winter El Niño teleconnection patterns. *Climate Dynamics*, *47*(12), 3737–3765. https://doi.org/10.1007/s00382-016-3039-1

Kanamitsu, M., Ebisuzaki, W., Woollen, J., Yang, S.-K., Hnilo, J. J., Fiorino, M., & Potter, G. L. (2002). NCEP–DOE AMIP-II Reanalysis (R-2). *Bulletin of the American Meteorological Society*, *83*(11), 1631–1644. https://doi.org/10.1175/bams-83-11-1631(2002)083<1631:nar>2.3.co;2

Kim, S. T., Lee, Y.-Y., Oh, J.-H., & Lim, A.-Y. (2021). Errors in the winter temperature response to ENSO over North America in seasonal forecast models. *Journal of Climate*, *34*(20), 8257–8271.

Kosaka, Y., & Nakamura, H. (2006). Structure and dynamics of the summertime Pacific–Japan teleconnection pattern. *Quarterly Journal of the Royal Meteorological Society*, *132*(619), 2009–2030. https://doi.org/10.1256/qj.05.204

Lau, K. H., & Lau, N. C. (1992). The energetics and propagation dynamics of tropical summertime synoptic-scale disturbances. *Monthly Weather Review*, *120*(11), 2523–2539. https://doi.org/10.1175/1520-0493(1992)120<2523:teapdo>2.0.co;2

Lau, N. C., Leetmaa, A., Nath, M. J., & Wang, H. L. (2005). Influences of ENSO-induced Indo-Western Pacific SST anomalies on extratropical atmospheric variability during the boreal summer. *Journal of Climate*, *18*(15), 2922–2942. https://doi.org/10.1175/jcli3445.1

Liu, Z., & Alexander, M. (2007). Atmospheric bridge, oceanic tunnel, and global climatic teleconnections. *Reviews of Geophysics*, *45*(2). https://doi.org/10.1029/2005rg000172

Lu, R. Y., Oh, J. H., & Kim, B. J. (2002). A teleconnection pattern in upper-level meridional wind over the North African and Eurasian continent in summer. *Tellus A: Dynamic Meteorology and Oceanography*, *54*(1), 44–55. https://doi.org/10.3402/tellusa.v54i1.12122

Rind, D., Chandler, M., Lerner, J., Martinson, D. G., & Yuan, X. (2001). Climate response to basin-specific changes in latitudinal temperature gradients and implications for sea ice variability. *Journal of Geophysical Research*, *106*(D17), 20161–20173. https://doi.org/10.1029/2000jd900643

Roeckner, E., Bäuml, G., Bonaventura, L., Brokopf, R., Esch, M., Giorgetta, M., et al. (2003). The atmospheric general circulation model ECHAM 5. Part I: Model description.

Sardeshmukh, P. D., & Hoskins, B. J. (1988). The generation of global rotational flow by steady idealized tropical divergence. *Journal of the Atmospheric Sciences*, *45*(7), 1228–1251. https://doi.org/10.1175/1520-0469(1988)045<1228:tgogrf>2.0.co;2

Seager, R., Harnik, N., Kushnir, Y., Robinson, W., & Miller, J. (2003). Mechanisms of hemispherically symmetric climate variability. *Journal of Climate*, *16*(18), 2960–2978. https://doi.org/10.1175/1520-0442(2003)016<2960:mohscv>2.0.co;2

Simmons, A. J., Wallace, J. M., & Branstator, G. W. (1983). Barotropic wave-propagation and instability, and atmospheric teleconnection patterns. *Journal of the Atmospheric Sciences*, *40*(6), 1363–1392. https://doi.org/10.1175/1520-0469(1983)040<1363:bwpaia>2.0.co;2

Su, H., & Neelin, J. D. (2002). Teleconnection mechanisms for tropical Pacific descent anomalies during El Nino. *Journal of the Atmospheric Sciences*, *59*(18), 2694–2712. https://doi.org/10.1175/1520-0469(2002)059<2694:tmftpd>2.0.co;2

Su, H., Neelin, J. D., & Meyerson, J. (2003). Sensitivity of tropical tropospheric temperature to sea surface temperature forcing. *Journal of Climate*, *16*(9), 1283–1301. https://doi.org/10.1175/1520-0442-16.9.1283

Tao, W., Huang, G., Wu, R., Hu, K., Wang, P., & Chen, D. (2016). Asymmetry in summertime atmospheric circulation anomalies over the northwest Pacific during decaying phase of El Niño and La Niña. *Climate Dynamics*, *49*(5–6), 2007–2023. https://doi.org/10.1007/s00382-016-3432-9

Trascasa-Castro, P., Maycock, A. C., Yiu, Y. Y. S., & Fletcher, J. K. (2019). On the linearity of the stratospheric and Euro-Atlantic sector response to ENSO. *Journal of Climate*, *32*(19), 6607–6626. https://doi.org/10.1175/jcli-d-18-0746.1

Trenberth, K. E., Branstator, G. W., Karoly, D., Kumar, A., Lau, N.-C., & Ropelewski, C. (1998). Progress during TOGA in understanding and modeling global teleconnections associated with tropical sea surface temperatures. *Journal of Geophysical Research*, *103*(C7), 14291–14324. Portico. https://doi.org/10.1029/97jc01444

Wang, X., & Yang, X.-Q. (2023). Amplified asymmetric impact of ENSO events on the wintertime Pacific-North American teleconnection pattern. *Geophysical Research Letters*, *50*(2), e2022GL100996. https://doi.org/10.1029/2022gl100996

Wang, Y., Hu, K., Huang, G., & Tao, W. (2021). Asymmetric impacts of El Nino and La Nina on the Pacific-North American teleconnection pattern: The role of subtropical jet stream. *Environmental Research Letters*, *16*(11), 114040. https://doi.org/10.1088/1748-9326/ac31ed

Wang, Y., Huang, G., Hu, K., Tao, W., Gong, H., Yang, K., & Tang, H. (2022a). Understanding the eastward shift and intensification of the ENSO teleconnection over South Pacific and Antarctica under greenhouse warming. *Frontiers in Earth Science*, *10*, 916624. https://doi.org/10.3389/feart.2022.916624

Wang, Y., Huang, G., Hu, K., Tao, W., Li, X., Gong, H., et al. (2022b). Asymmetric impacts of El Niño and La Niña on the Pacific–South America teleconnection pattern. *Journal of Climate*, *35*(6), 1825–1838. https://doi.org/10.1175/jcli-d-21-0285.1

Watanabe, M., & Kimoto, M. (2000). Atmosphere-ocean thermal coupling in the North Atlantic: A positive feedback. *Quarterly Journal of the Royal Meteorological Society*, *126*(570), 3343–3369. https://doi.org/10.1002/qj.49712657017

Xie, S.-P., Hu, K., Hafner, J., Tokinaga, H., Du, Y., Huang, G., & Sampe, T. (2009). Indian Ocean capacitor effect on Indo–Western Pacific climate during the summer following El Niño. *Journal of Climate*, *22*(3), 730–747. https://doi.org/10.1175/2008jcli2544.1

Yeh, S.-W., Cai, W., Min, S. K., McPhaden, M. J., Dommenget, D., Dewitte, B., et al. (2018). ENSO atmospheric teleconnections and their response to greenhouse gas forcing. *ENSO Atmospheric Teleconnections and Their Response to Greenhouse Gas Forcing*, *56*(1), 185–206. https://doi.org/10.1002/2017rg000568

Yiu, Y. Y. S., & Maycock, A. C. (2020). The linearity of the El Nino teleconnection to the Amundsen Sea region. *Quarterly Journal of the Royal Meteorological Society*, *146*(728), 1169–1183. https://doi.org/10.1002/qj.3731

Zhou, W., Yang, D., Xie, S.-P., & Ma, J. (2020). Amplified Madden–Julian oscillation impacts in the Pacific–North America region. *Nature Climate Change*, *10*(7), 654–660. https://doi.org/10.1038/s41558-020-0814-0